AUTOMATIC VEHICLE DETECTION IN SATELLITE IMAGES

J. Leitloff [1], S. Hinz[2], U. Stilla[1]

[1] Photogrammetry and Remote Sensing, [2] Remote Sensing Technology
Technische Universitaet Muenchen, Arcisstrasse 21, 80333 Muenchen, Germany
{jens.leitloff, stefan.hinz, stilla}@bv.tum.de

KEY WORDS: Urban, Feature extraction, Edge detection, Optical Satellite Imagery, Quickbird

ABSTRACT:
Vehicle detection is motivated by different fields of application, e.g. traffic flow management, road planning or estimation of air and noise pollution. Therefore, an algorithm that automatically detects and counts vehicles in air- or space-borne images would effectively support these traffic-related analyses in urban planning. Due to the small vehicle size in satellite images detection of single vehicles would deliver ambiguous results. Hence, our scheme focuses primarily on the extraction of vehicle queues, as the pattern of a queue makes it better distinguishable (as a whole) from similar objects. Hypotheses for queues are generated by sophisticated extraction of ribbons. Within these ribbons single vehicles are searched for by least-squares fitting of Gaussian kernels to the width and contrast function of a ribbon. Based on the resulting parameter values, false and correct hypotheses are discerned. The results show that the analysis of width and contrast information using least square optimization is able to extract single vehicles from queues with high correctness. Still, the completeness of the overall extraction is relatively low, since only queues can be extracted but no isolated vehicles. The results clearly show that the approach is promising but further improvements are necessary to achieve a higher completeness.

1. INTRODUCTION

1.1 Motivation

There is an increasing demand for traffic monitoring of densely populated areas. The traffic flow on main roads can partially be measured by fixed installed sensors like induction loops, bridge sensors and stationary cameras. Traffic on smaller roads – which represent the main part of urban road networks – is scarcely monitored and information about on-road parked vehicles is not collected. Wide-area images of the entire road network can complement these selectively acquired data. New optical sensor systems on satellites, which provide images of 1-meter resolution or better, e.g. Ikonos and QuickBird, make this kind of imagery available. Hence new applications like traffic monitoring and vehicle detection from these images have achieved considerable attention on international conferences, e.g. (Bamler and Chiu, 2005; Heipke et al., 2005; Stilla et al., 2005). The presented approach focuses on the detection of single vehicles by extracting of vehicle queues from satellite imagery.

1.2 Related work

Depending on the used sensors and the resolution of the imagery different approaches (Stilla et al., 2004) have been developed in the past. The extraction of vehicles from images with a resolution of about 0.15 m has already been comprehensively tested and delivers good results in many situations. Available approaches either use implicit or explicit vehicle models (Hinz, 2003). The appearance-based, implicit model uses example images of vehicles to derive gray-value or texture features and their statistics, which are assembled in vectors. These vectors are used as reference to test computed feature vectors from image regions. Since the implicit model classification uses example images the extraction results depend strongly on the choice of representative images.
Approaches using an explicit model describe vehicles in 2 or 3 dimensions by filter or wire-frame representations. The model is then either matched "top-down" to the image or extracted image features are grouped "bottom-up" to create structures similar to the model. A vehicle will be declared as detected, whenever there is sufficient support of the model found in the image. These approaches deliver comparable or even better results than approaches using implicit models but are hardly applicable to satellite imagery since there vehicles only appear as blobs without any prominent sub-structures (see Fig. 1).

Three different methods for vehicle detection from simulated satellite imagery of highway scenes are tested in (Sharma, 2002). The gradient based method and the method using Bayesian Background Transformation (BBT) deliver the best number of vehicle counts compared to ground truth. Since the number of false detections is lower using BBT, this method is more reliable. The performance of the third method using Principal Component Analysis (PCA) varies significantly with the noise level of the image. Furthermore, the method gives the lowest vehicle count. A manually created background image is mandatory for the PCA and BBT method, which requires extensive interactive work. Consequently, the approaches can hardly be generalized and are limited to images of the same scene.
In (Gerhardinger et al., 2005) the commercial software *Features Analyst®* is used to implement an iterative learning approach by analyzing the spectral signature and the spatial context. The authors report that good results can be achieved if a very
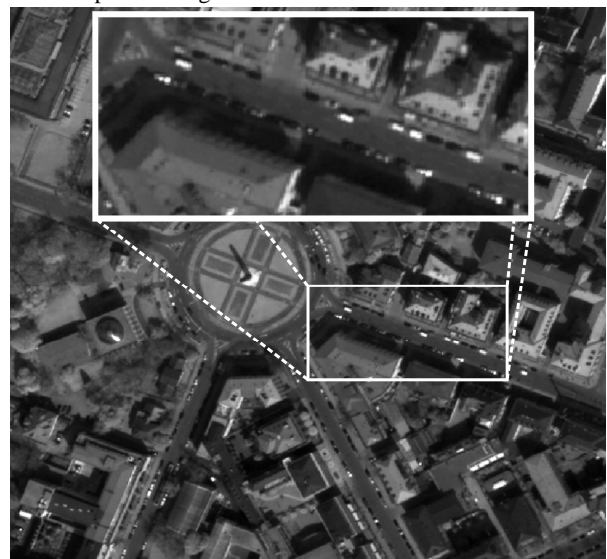
Figure 1: Appearance of vehicles in optical high-resolution satellite imagery (Quickbird), GSD = 0.6 m

accurate road GIS is available. However, this had to be derived by manual digitalization in their case.

An encouraging approach for single vehicle detection is presented in (Jin and Davis, 2004). First, they use morphological filtering for a rough distinction between vehicle pixels and non-target pixels, which are similar to vehicles. Then a morphological shared-weight neural network is used for extraction. The approach achieves good performance values under the condition that vehicles appear isolated. However, the approach is not designed for vehicle queues or traffic jams (Jin and Davis, 2004).

The last mentioned approaches are designed for a resolution coarser than 0.5 m and limit their search space to roads and parking lots using GIS information. By this, the number of false alarms is significantly decreased.

In dense traffic situations, traffic jams or parking lots, car groupings show quite evident regularities (see e.g. Fig. 1). Exploiting the knowledge about these repeating occurrences and the fact that cars rarely occur isolated is also referred to as global modeling in the filed of vehicle detection. Vehicle hypotheses extracted by a neural network classifier (Ruskoné et al., 1996) or a "spot detector" (Michaelsen & Stilla, 2001) are collinearly grouped into queues while isolated vehicle hypotheses are rejected. Hinz & Stilla (2006) use a differential geometric blob detector for an initial extraction of car candidates followed by a modified Hough transform for accumulating global evidence for car hypotheses. Since these grouping schemes select hypotheses but do not add new hypotheses, these approaches need an over-segmentation as initial input. They are designed for medium resolution images of approximately 0.5m ground sampling distance (GSD).

When high resolution imagery is available a more promising strategy is to focus on reliable hypotheses for single vehicles first and complete the extraction afterwards by searching for missing vehicles in gaps of a queue using a less constrained vehicle model (Hinz, 2003). By this, not only queues but also isolated cars can be extracted as long as they belong to the set of reliable hypotheses.

One of the few approaches focusing directly on vehicle queues – in particular military convoys – is presented in Burlina et al. (1997). They extract repetitive, regular object configurations based on their spectral signature. In their approach the search space is limited to roads and parking lots using accurate GIS-information. This seems necessary since the spectrum will be heavily distorted, if adjacent objects gain much in influence – even if the spectrum is computed for quite small images patches.

1.3 Overview

Figure 3 shows the overall structure of our approach which is separated into three processing stages. In the pre-processing step (Fig. 2 I), GIS data is used to determine Regions of Interest (ROI). Afterwards we use a differential geometric approach followed by some post-processing to extract linear features as hypotheses of the queues (Sect. 2.2 and 2.3; Fig. 2 II). Finally, we determine single vehicles from these hypotheses by analyzing the width and contrast function using a least squares optimization (Sect.2.4; Fig. 2 III).

2. QUEUE DETECTION

In Sect. 2.1 the used model will be presented. Sect. 2.2 describes the extraction of vehicle queues using sophisticated line extraction. Then a number of attributes are calculated (Sect. 2.3). The attributes are analyzed and checked for consistency to
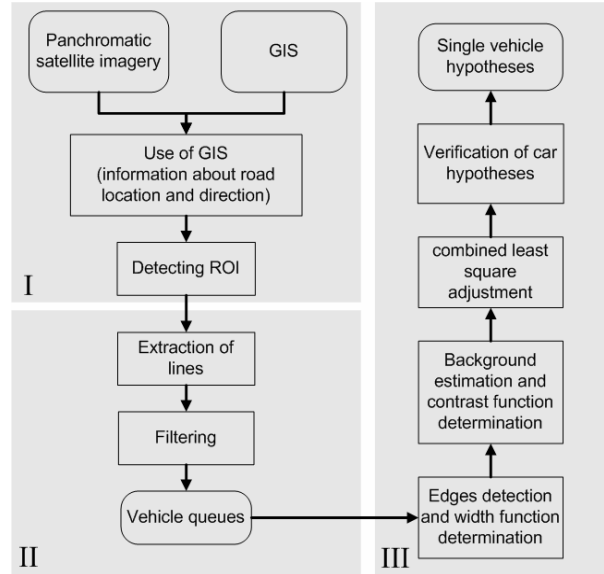

Figure 2: Processing Scheme

verify or falsify single vehicle hypotheses. This is done by a least square adjustment (discussed in Sect. 2.4) and by an iterative constrained search (see Sect. 2.5).

2.1 Model of vehicle queues

Generally, a vehicle queue is defined as ribbon with distinct symmetries along and across its local orientation. Basically, the model is similar to that defined in (Hinz, 2003); though, since this model is originally designed for aerial images, a number of modifications regarding the significance of different features have been applied:

A vehicle queue

- must have sufficient length, bounded width and low curvature;
- shows a repetitive pattern along the centerline, both in contrast and width (Fig. 3a), while length and width of the individual replica correspond to vehicle dimensions;
- collapses to a line in Gaussian scale space, i.e. when smoothing the image accordingly (Fig. 3b).

Please note that this queue model differs from the above mentioned approaches in a way that – in particular through the scale-space description – the queue is modeled as a unique structure and not just as a composite of its underlying, smaller elements. At first glance, this seems of less importance. Still, it provides the basis for detecting a queue hypothesis as a whole
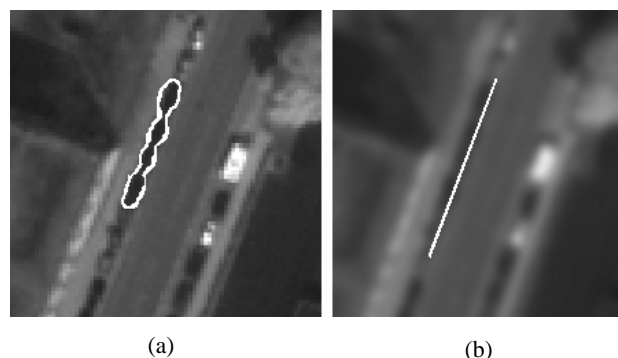

| (a) | (b) |

Figure 3: Queue model. a) original image, b) smoothed image

(even though at a coarser scale) rather than constructing it from smaller elements. Thereby global knowledge can be incorporated from the very beginning of the extraction.

2.2 Extraction of vehicle queues

Figure 4 illustrates the a priori information about road location and direction taken from a national core database. The positional accuracy is known to be approximately 2m. Neither the road sides are contained in the database nor the position of the individual lanes. Hence, the road width needs to be estimated from attributes like the number of lanes or the average width per road segment. Thus the generated regions of interest (ROI) can only be regarded as an approximation of the true road area.

Line extraction is carried out by applying the differential geometric approach of Steger (1998). This algorithm is primarily based on the computation of the second image derivatives, i.e. the local curvatures of the image function. Parameters for the line extraction are chosen corresponding to the vehicle geometry (vehicle width: w) and radiometry (expected contrast to road: c).

Thus, the necessary input parameters for line extraction σ, t_L and t_H can be calculated as follows:

$$\sigma = \frac{w}{2\sqrt{3}} \qquad t = c\frac{-w}{\sqrt{2\pi} \cdot \sigma^3} e^{-\frac{1}{2}\left(\frac{w}{2\sigma}\right)^2} = c\frac{-\sqrt{6} \cdot 12}{\sqrt{\pi} \cdot w^2} e^{-\frac{3}{2}} = c \cdot a$$

$$t_L = c_L \cdot a \qquad t_H = c_H \cdot a$$

where σ defines the preliminary smoothing factor, calculated from the maximum expected width (e.g. 2.5 meter). t_L and t_H define the hysteresis thresholds for the second partial derivative of the image at each point. If the value exceeds t_H a point is immediately accepted as line point. All points where the second derivative is smaller than t_L are rejected. Points with a second derivative between t_H and t_L are accepted if they can be connected to already accept points. In order to achieve initial hypotheses, the parameters for c_L (minimum contrast to be accepted) and c_H (contrast for queues definitely to accept) are chosen quite relaxed.

Additionally, the line extraction algorithm is supported by morphologically filtering the image with a directional

Figure 4: Regions of Interest

**Figure 5:** Resulting lines after merging, smoothing and filtering.

rectangular structuring element oriented along the particular road segment. In doing so the queues are enhanced and disturbing substructures in bright cars are almost completely removed. The relaxed parameter settings lead to a huge number of false hypotheses but also return most of the promising hypotheses for vehicle queues. However, since the line extraction requires a minimum contrast between vehicles and the road surface, gray vehicles can not be extracted reliably, as they hardly emerge from their surroundings.

Bright and dark lines are extracted separately. They are connected if they fulfill some distance and collinearity criteria. In our case a maximum distance of one vehicle length must not be exceeded. Additionally, one has to keep in mind that the merging of parallel lines would lead to significant positional errors and is therefore prevented. The final processing steps consist of geometrical smoothing by polygonal approximation, resampling (Ramer, 1972) and testing all resulting lines against a minimum length threshold and an upper limit for direction differences to the road. Results of the merging and filtering steps are illustrated in Fig. 5.

2.3 Determining queue width and contrast

After extracting lines as medial axes of a ribbon, width and contrast functions are determined. The algorithm to find the ribbon width in each line point is based on profiles spanned perpendicular to the local line direction, and determining each profile's gray values by bilinear interpolation. Then, for each profile, local maxima are determined with sub-pixel precision by fitting a second-order polynomial to the first derivative of the gray value profile in each profile point. The first maximum value found on either side of centerline is supposed to correspond to the vehicle boundary, i.e., the distance between the two maxima yields the queue width. If no maximum is found, gaps in the width function are closed afterwards by linear inter- or extrapolation.

Results of width determination are illustrated in Fig. 6. It can be seen that most edges correspond to vehicle sides. Because of weak contrast between vehicles and road surface a number of outliers are present, which are to remove by median filtering the width function.
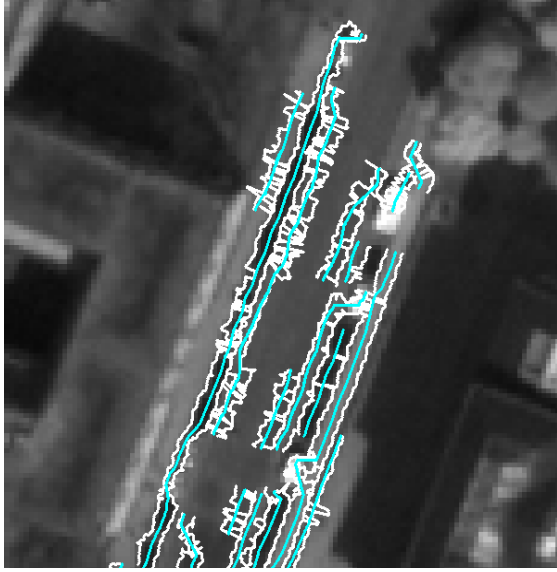
**Figure 6:** Extracted ribbons: medial axis (cyan) and width function (white).

One can see that most edges correspond to vehicle sides. However, since the gradient image has quite weak contrast, the edges extraction results show also some irregularities, i.e. noisy boundaries. Therefore smoothing of the extracted edges is useful to reduce the number of outliers.

Usually the irregularities are caused by other edges nearby the vehicle queue. In future implementations we intend to detect such outliers by a more sophisticated shape analysis of the boundary functions.

To determine the contrast function of a ribbon, a reference gray value outside the vehicle regions must be defined. The actual gray values in the direct neighborhood of a vehicle, however, are often influenced by adjacent objects or shadows and are therefore no reliable estimates of the reference gray value. A better way to determine the contrast function is to estimate the median road surface brightness in the neighborhood of a vehicle queue and use this estimate as reference gray value. Assuming that – despite of the presence of some vehicles – the most frequent gray values in the RoI represent the road surface, and further assuming that in the center of a road less disturbances by vehicles and shadows occurs than at the road sides, the following simple procedure has been implemented to compute the road surface brightness:

- project the start and end point of each extracted centerline onto the GIS road axis, thereby defining the relevant road section
- dilate this section by approximately the width of one lane
- calculate the median gray value of this image region in order to estimate the road surface brightness

Since the gray values along the medial axes have already been extracted, the contrast function simply results from the absolute difference of these values and the reference gray value. In Fig. 7 examples of width and contrast function of a ribbon are shown. It furthermore illustrates that both functions show mutually correlated repetitive patterns which will be used to detect single vehicles.
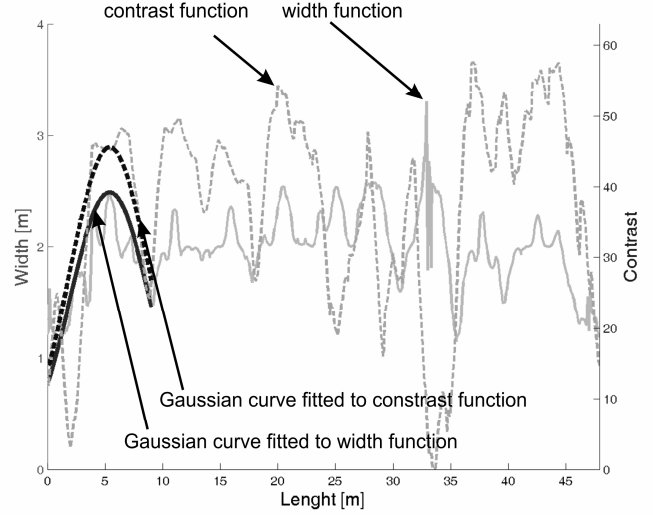
Figure 7: Width and contrast function of a ribbon

2.4 Single vehicle determination by least squares optimization

For extraction of single vehicles from a ribbon, Gaussian kernels are fitted to the width and contrast function (Fig. 7). Of course, different kernels like a second-order polynomial could be used instead. However, the estimated parameters of a fitted Gaussian kernel relate not only to the desired vehicle dimensions but also allow to establishing a link to the particular scale used for line extraction in Sect. 2.2. – especially the Gaussian kernels fitted to the contrast function. The rationale of the procedure outlined in the following should thus be understood as an attempt to embed the vehicle detection into the same scale-space framework as the line extraction approach.

The calculation of the unknown parameters of each Gaussian kernel is done by a least squares fit. The notation corresponds to the work of Mikhail (1976).

The functional model of a Gaussian function to fit to a predefined interval of the width functions has the following form:

$$w(a_w, \sigma_w, \mu) = \frac{a_w}{\sqrt{2\pi}\sigma_w} e^{-\frac{1}{2}\left(\frac{x-\mu}{\sigma_w}\right)^2} \quad (1)$$

with $w(...)$ width as function of a_w, σ_w and μ
   a_w the amplitude of the fitted Gaussian kernel
   σ_w second-order moment of the Gaussian kernel
   μ first-order moment of the Gaussian kernel, i.e. the position of maximum amplitude
   x position of w along the interval under investigation

The functional model for the contrast function is quite similar:

$$c(a_c, \sigma_c, \mu) = \frac{a_c}{\sqrt{2\pi}\sigma_c} e^{-\frac{1}{2}\left(\frac{x-\mu}{\sigma_c}\right)^2} \quad (2)$$

with $c(...)$ contrast as function of a_c, σ_c and μ
   a_c the amplitude of the fitted Gaussian curve
   σ_c second-order moment of the Gaussian curve
   μ first-order moment of the Gaussian kernel, i.e. the position of maximum amplitude

x — position of value c along the interval under investigation

Since a vehicle should yield the maximum of both width and contrast function at the same position, μ is a shared parameter in both functions. Fig. 7 illustrates an example of the contrast and the width signal. The fitted Gaussian curves for the first interval are also included. These intervals are defined by two consecutive minima in a smoothed version of the function. It is also apparent from Fig. 7 that additionally introducing σ as shared parameter would not lead to satisfactory results. The pronounced differences between the shapes of the two functions would cause the accuracy of the estimated unknown σ to drop down significantly.

The unknown parameters of the functional model (1) and (2) are summarized in the vector $\boldsymbol{x}$:

$$\boldsymbol{x}^T = \begin{pmatrix} a_w & \sigma_w & \mu & a_c & \sigma_c \end{pmatrix}$$

It is easy to see that the functions (1) and (2) are nonlinear. Therefore the determination of the unknown parameters is an iterative process, where $\boldsymbol{x}$ needs to be calculated by (see (Mikhail, 1976):

$$\boldsymbol{x} = \boldsymbol{x}^0 + \boldsymbol{\Delta} \qquad (3)$$

and

$$\boldsymbol{\Delta} = \left(\boldsymbol{B}^T \boldsymbol{B}\right)^{-1} \boldsymbol{B}^T \left(\boldsymbol{l} - \boldsymbol{f}\left(\boldsymbol{x}^0\right)\right)$$

assuming the observations to be uncorrelated and of equal accuracy, i.e. neglecting the weighting matrix $\boldsymbol{W}$. Vector $\boldsymbol{l}$ contains the observations of the current interval and $\boldsymbol{f}(\boldsymbol{x}^0)$ the width and contrast function derived from the initial values $\boldsymbol{x}^0$. $\boldsymbol{\Delta}$ are the corrections to the initial values and $\boldsymbol{B}$ is the Jacobian matrix containing the partial derivatives with respect to the unknowns of the Gaussian kernels.

The vectors $\boldsymbol{l}$ and $\boldsymbol{f}(\boldsymbol{x}^0)$ are defined by:

$$\boldsymbol{l}^T = \begin{pmatrix} w_f \cdots w_l\, c_f \cdots c_l \end{pmatrix}$$

$$\boldsymbol{f}(\boldsymbol{x}^0)^T = \left(w\left(a_w^0, \sigma_w^0, \mu\right)_f \cdots w\left(a_w^0, \sigma_w^0, \mu\right)_l\, c\left(a_c^0, \sigma_c^0, \mu\right)_f \cdots c\left(a_c^0, \sigma_c^0, \mu\right)_l \right)$$

where indices f (first value) and l (last value) indicate the boundaries of the interval under investigation.

Values for $\boldsymbol{x}^0$ are chosen considering that:

- μ^0 corresponds to the position of the maximum of the current interval
- a_c^0 is the contrast value at position μ^0
- $\sigma_w^0 = \sigma_c^0$ is chosen according to the supposed vehicle length
- a_w^0 can be calculated by $a_w = w_\mu \cdot \sqrt{2\pi} \cdot \sigma_w$ where w_μ is the width at maximum μ

Now the unknowns $\boldsymbol{x}$ can be calculated according to Equ.3. If the L1-norm $\left\| \boldsymbol{x} - \boldsymbol{x}^0 \right\|$ is greater than a predefined threshold, $\boldsymbol{x}^0$ is replaced by $\boldsymbol{x}$ and $\boldsymbol{\Delta}$ will be calculated again until convergence or after a maximum number of iterations is reached.

Furthermore the accuracy of the unknowns can be obtained from the diagonal of the $\boldsymbol{C}_{xx}$ matrix, which is calculated by:

$$\boldsymbol{C}_{xx} = \hat{\sigma}_0^2 \cdot \boldsymbol{Q}_{xx} = \hat{\sigma}_0^2 \cdot \left(\boldsymbol{B}^T \boldsymbol{B}\right)^{-1}$$

with

$$\hat{\sigma}_0^2 = \frac{\boldsymbol{v}^T \boldsymbol{v}}{n-u} .$$

Here n is the number of observations, u is the number of unknown parameters (here 5) and $\boldsymbol{v}$ contains the observations' residuals, which are calculated by:

$$\boldsymbol{v} = \boldsymbol{B} \cdot \boldsymbol{\Delta} - \left(\boldsymbol{l} - \boldsymbol{f}\left(\boldsymbol{x}^0\right)\right)$$

If the width and the contrast functions exhibit the expected repetitive pattern, only a few iterations are necessary.

As final result of the least squares adjustment, we obtain the parameters describing a fitted Gaussian kernel for a given interval including their accuracies. Thresholds are applied to these parameters to discern false and correct hypotheses. The required thresholds were acquired from test datasets.

In some cases multiple detections of the same vehicle occur due to neighboring ribbons. Therefore, an overlap analysis is carried out in which all overlapping (or nearby) hypotheses are mutually tested for consistency. In case of conflicts the worse hypothesis is rejected.

2.5 Single vehicle determination by iterative constrained search

A second method to find single vehicles also uses the appearance of significant repetitive patterns in the width function (Figure 8). Here, maximum values in this function are assumed to approximately represent the centers of single vehicles whereas minimum values are assumed to represent gaps between two vehicles of a queue.

The following parameters are used:

- v_{min} ... minimum length of a single vehicle (SV) and search interval (SI)
- v_{max} ... maximum length of SV and SI
- l_{min} ... position of the minimum width within SI
- l_{max} ... position of the maximum width within SI
- d ... distance between l_{min} and l_{max}

A vehicle hypothesis is generated if the following condition is fulfilled: $\dfrac{v_{min}}{2} \le d \le \dfrac{v_{max}}{2}$
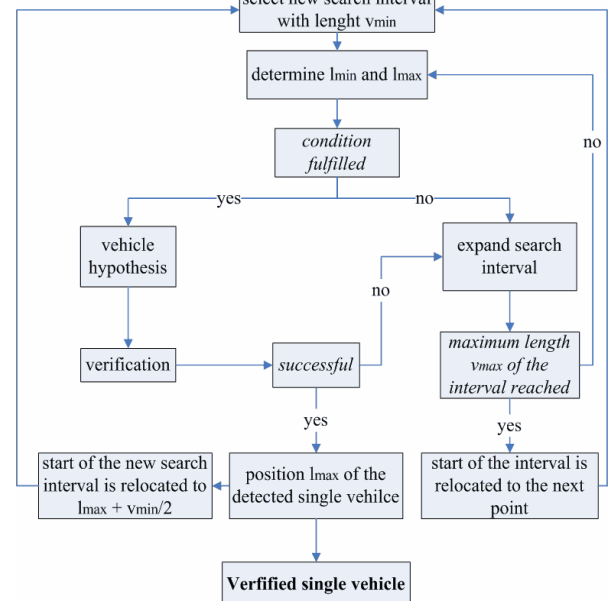

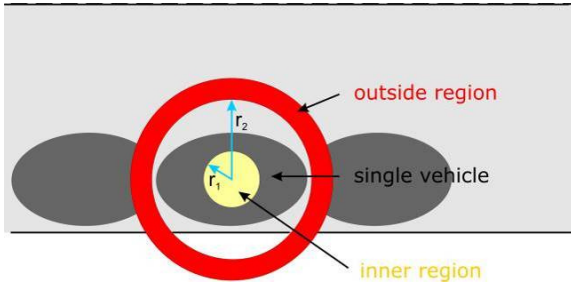**Figure 8**: Concepts of width functions' analysis

Figure 9: Verification

Figure 8 shows the flow chart of the width analysis scheme. Essentially, this algorithm tries to find local maxima and minima in the noisy width function and place the vehicle positions in such a way that vehicle hypotheses do not overlap.

It is possible that more than one hypothesis is found for a single vehicle. This is caused by two or more maxima in the width function within size of a vehicle. Therefore we control the space between two hypotheses not to fall below a certain minimum distance. If more than one hypothesis is found within this minimum distance, the hypothesis with the highest maxima in the width function will be verified.

Unlike the method described in Sect. 2.4, the contrast function is not used here. Rather, the contrast of the vehicle and the adjacent road surface is used for a simple verification after a hypothesis has been generated. Here the difference of the median gray values of the inner and the outer region is calculated (see Figure 9).

3. RESULTS

In Figures 10 and 11, results achieved with the extraction approach from Sect. 2.4 are shown. Therefore, we processed an image scene covering an area of 0.1 sq. km. Cyan ellipses correspond to correct extractions, white ellipses represent misdetections. As can be seen, the ellipses of the correct extractions coincide quite well with the actual vehicles, clearly indicating that the fitting procedure works reliably. This is a very encouraging result, especially when recalling Figure 7, which gives an impression on the "noisiness" of the contrast and width function.

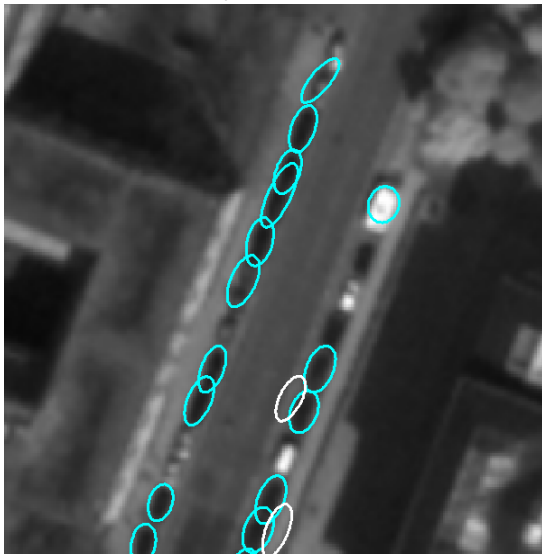However, there are also a number of misdetections, in particular at side-walks when dark objects are on either side of the side-walk (see e.g. Fig. 11). Such failures could be overcome, for instance, by a more detailed analysis of neighborhood relations of extracted vehicles. A constellation as achieved for the right queue in Fig. 10 is very unlikely to happen; four vehicles are almost perfectly aligned in a row while each of the other two vehicles is located on a different side of this row. Incorporating this kind of reasoning into the approach would allow to further reducing the misdetection rate.

Fig. 10 and 11 also show that a number of cars are not extracted, i.e. the completeness of this approach is quite fair. However, one has to keep in mind that vehicles do not always appear as queues and, furthermore, that the line extraction does not extract all existing queues. In fact, tests have shown that approximately 60% of all vehicles are contained in the ribbons that serve as initial hypotheses. Besides this, also the edge detection procedure for determining a ribbon's width could be improved to support convergence of the least squares adjustment.

For numerical evaluation, manually created reference data sets have been utilized and the well-known criteria "correctness" and "completeness" values are calculated as evaluation measures:

$$correctness = \frac{TP}{TP + FP}$$

$$completeness = \frac{TP}{TP + FN}$$

with   TP   true positives
         FP   false positives
         FN   false negatives

Here true positives are correctly extracted vehicles, false positives are misdetections, and false negatives are missed vehicles with respect to the reference data. Table 1 summarizes the evaluation results depending on the type of reference data and the used method:

a) all vehicles using least squares adjustment
b) all vehicles using iterative constrained search
c) only bright and dark vehicles, i.e. without gray vehicles (using least squares adjustment)
d) only bright and dark vehicles, i.e. without gray vehicles (using iterative constrained search)

Gray vehicles have been excluded from the reference in b) and d) since they almost show no contrast to their surroundings. We would like to mention in addition that the acquisition of
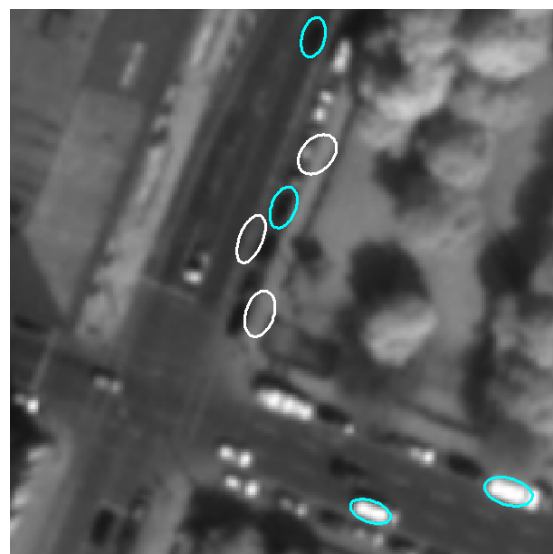

Figure 10: Extraction results I

Figure 11: Extraction results II

reference data for some vehicles is certainly not free of errors. Even a human observer is sometimes not able to identify all vehicles in an image scene with high confidence. Therefore our reference data can only be considered as a very good approximation of real "ground-truth".

It can be seen from Table 1, that on one hand both approaches deliver comparable results, although the iterative constrained search generally achieves higher completeness with better correctness at the same time. On the other hand the single vehicle determination by least square optimization gives statistical accuracy of all hypotheses. It is planned to use these values for internal evaluation, which is supposed to increase performance and reliability.

	Reference data			
	(a)	(b)	(c)	(d)
Completeness [%]	31.1	34.1	36.1	40.3
Correctness [%]	73.5	76.0	70.5	72.3

Table 1: Numerical Evaluation

Despite the weak completeness, the good correctness of the extracted vehicles allows to use them as starting point for searching additional vehicles. Therefore the next steps of implementation will include the search for isolated vehicles using the information from the previous queue detection. Preliminary investigations using a differential blob detector (Hinz, 2005) for accomplishing this task have already taken out.

Concluding the discussion, vehicles with good or even medium contrast to the road surface can be extracted very accurately. Furthermore, the results show that the analysis of width and contrast information using least square optimization allows to extracting single vehicles from queues with high correctness. Still, the completeness of the overall extraction is relatively low, since only queues can be extracted but no isolated vehicles. The results clearly show that the approach is promising but further improvements are necessary to achieve a higher completeness.

REFERENCES

Bamler R., Chiu, S., 2005. Spaceborne Traffic Monitoring from SAR and Optical Data (Jointly Organized with ISPRS WGII/5). Session at IGARSS'05 (on CD)

Burlina, P., Chellappa, R. and Lin, C. (1997): A Spectral Attentional Mechanism Tuned to Object Configurations, IEEE Transactions on Image Processing 6, 1117–1128.

Gerhardinger, A., Ehrlich, D., Pesaresi, M., 2005. Vehicle detection from very high resolution satellite imagery. International Archives of Photogrammetry, Remote Sensing and Spatial Information Sciences 36 (Part 3/W24), 83-88.

Heipke, C., Jacobsen, K., Gerke, M. (eds), 2005. High-resolution earth imaging for geospatial information. International Archives of Photogrammetry and Remote Sensing. Vol 36 Part 1 W3 (on CD)

Hinz, S., 2003. Integrating local and global features for vehicle detection in high resolution aerial imagery. International Archives of Photogrammetry, Remote Sensing and Spatial Information Sciences 34 (Part 3/W8), 119-124.

Hinz, S., 2005. Fast and Subpixel Precise Blob Detection and Attribution . Proceedings of ICIP 05, Genua, Sept. 11-14 2005.

Hinz, S., Stilla, U., 2006. Car detection in aerial thermal images by local and global evidence accumulation. Pattern Recognition Letters 27, 308-315.

Jin X., Davis, C.H., 2004. Vector-guided vehicle detection from high-resolution satellite imagery. In: Proc. IEEE International Geoscience and Remote Sensing Symposium (IGARSS '04), Vol. 2, Anchorage, USA-AK, 20-24 September 2004, 1095 – 1098.

Michaelsen, E., Stilla, U., 2001. Estimating Urban Activity on High-Resolution Thermal Image Sequences Aided by Large Scale Vector Maps. In: Proc. IEEE/ISPRS Joint Workshop on Remote Sensing and Data Fusion over Urban Areas, Rome, Italy, 8-9 November 2001, 25-29

Mikhail, E. M., 1976. Observations and least squares. IEP – A Dun-Donnelly Publisher, Copyright: Thomas Y. Crowell Company Inc., New York

Ramer, U. (1972): An Iterative Procedure for the Polygonal Approximation of Plane Curves, Computer Graphics and Image Processing 1, 244-256.

Ruskoné, R., Guiges, L., Airault, S., Jamet, O., 1996. Vehicle detection on aerial images: A structural approach. In: Kropatsch, G. (Eds.), Proc. 13th International Conference on Pattern Recognition (ICPR'96), Vol. 3, IEEE Computer Society Press, Vienna, Austria, 25 -29 August 1996, 900-903.

Sharma, G., 2002. Vehicle detection and classification in 1-m resolution imagery. MSc Thesis, Ohio State University, Columbus, USA-OH.

Steger, C., 1998. An Unbiased Detector of Curvilinear Structures. IEEE Transactions on Pattern Analysis and Machine Intelligence 20 (2), 113-125.

Stilla, U., Michaelsen, E., Soergel, U., Hinz, S., Ender, J., 2004. Airborne monitoring of vehicle activity in urban areas. International Archives of Photogrammetry, Remote Sensing and Spatial Information Sciences 35 (Part B3), 973-979.

Stilla, U., Rottensteiner F., Hinz. S. (Eds.), 2005. Object Extraction for 3D City Models, Road Databases, and Traffic Monitoring - Concepts, Algorithms, and Evaluation (CMRT05), Int. Archives of Photogrammetry, Remote Sensing and Spatial Information Sciences, Vol. XXXVI, Part 3/W24